Sun et al. Nanoscale Research Letters (2016) 11:110
DOI 10.1186/s11671-016-1326-8

Nanoscale Research Letters
a SpringerOpen Journal

NANO EXPRESS Open Access

Synthesis of Nitrogen and Sulfur Co-doped Carbon Dots from Garlic for Selective Detection of Fe^{3+}

Chun Sun[1], Yu Zhang[1*], Peng Wang[3], Yue Yang[1], Yu Wang[2*], Jian Xu[4], Yiding Wang[1] and William W. Yu[1]

Abstract

Garlic was used as a green source to synthesize carbon dots (CDs) with a systematic study of the optical and structure properties. Ethylenediamine was added into the synthesis to improve the photoluminescence quantum yield (PL QY) of the CDs. Detailed structural and composition studies demonstrated that the content of N and the formation of C–N and C=N were critical to improve the PL QY. The as-synthesized CDs exhibited excellent stability in a wide pH range and high NaCl concentrations, rendering them applicable in complicated and harsh conditions. Quenching the fluorescence of the CDs in the presence of Fe^{3+} ion made these CDs a luminescent probe for selective detection of Fe^{3+} ion.

Keywords: Carbon dots, Garlic, Ion detection

Background

Fluorescent materials have drawn considerable attention owing to their potential applications in a variety of fields, such as bioimaging, optoelectronic devices, and sensing [1–7]. Semiconductor quantum dots (QDs) have become one of the most promising nanomaterials due to their high photostability, large molar extinction coefficients [8, 9], high photoluminescence quantum yields (PL QYs), and size-tunable emission [10]. However, these popular QDs have raised concerns over serious toxicity and environmental hazard [11]. In addition, their superior optical features are usually applied in organic solvents, thus restricting their direct analytical and biological applications to a great degree. Various methods have been applied to make these luminescent QDs water-soluble, such as surface passivation with hydrophilic protective layers [12–14] and water-phase synthesis. However, these protocols are compromised at the expense of reducing the PL QYs and the time-consuming, complicated, expensive processes [15].

Carbon nanoparticles, or carbon dots (CDs) are free of toxic elements. They have recently emerged as the most attractive candidates to replace QDs with outstanding advantages, such as the excellent water solubility, strong luminescence, high biocompatibility, and good photostability [16–23].

Typically, the strategies for synthesizing CDs can be divided into two major categories: top-down and bottom-up methods. Top-down methods consist of laser ablation [24], arc discharge [25], and chemical oxidation [26], where the CDs are formed by cutting a large carbon structure into small pieces. In bottom-up methods, the CDs are synthesized by carbonization of organic molecular precursors through solvothermal methods [27, 28], microwave treatment [29], ultrasonic-assisted synthetic methods [30], and so on. Among them, the top-down methods often require sophisticated and expensive energy-consuming equipment [31]. The ultrasonic-assisted synthetic methods rely on strong acids or bases [30]. Typically, CDs can be synthesized within minutes by microwave irradiation, while they suffer from uncontrollable reaction conditions. The hydrothermal route is mostly preferred because of its simplicity, controlled reaction conditions, and cost-effectiveness [31].

Despite several advancements in the field of CDs synthesis [27, 28, 32], there are some by-products using conventional chemicals, which do not meet the standard

* Correspondence: yuzhang@jlu.edu.cn; yu.wang@upol.cz
[1]State Key Laboratory on Integrated Optoelectronics, and College of Electronic Science and Engineering, Jilin University, Changchun 130012, China
[2]Department of Physical Chemistry, Regional Centre of Advanced Technologies and Materials, Faculty of Science, Palacký University in Olomouc, Šlechtitelů 27, 783 71 Olomouc, Czech Republic
Full list of author information is available at the end of the article

of non-toxicity. Besides, expensive precursors and complicated post-treatment processes for surface passivation also hinder the broad application of CDs. Therefore, many efforts have been made for the preparation of CDs using easily accessible and natural precursors as starting materials. For example, milk [33], potato [34], grape juice [35], lime juice [36], orange juice [37], pomelo peel [38], grass [39], willow bark [40], and even waste biomass [41] have been used as the green sources for CDs. Nevertheless, it still remains a major challenge to achieve biomass-derived CDs with high PL QYs.

Recently, heteroatom-doped CDs have been reported with enhanced optical and electronic properties. It has revealed that heteroatom doping plays a vital role in tuning compositions and structures of CDs [42, 43]. Particularly, there were intensive investigations of nitrogen-doped CDs [44], while nitrogen and sulfur co-doped CDs were rarely reported. Garlic is a cheap, easily available natural condiment, containing carbohydrate, proteins, and thiamine, and abundant in carbon, nitrogen, and sulfur elements. Consequently, dehydration, polymerization, carbonization, and passivation may involve in the formation of CDs under high temperature and pressure during the hydrothermal treatment [22, 23]. We report herein a green synthetic method for N and S co-doped CDs from garlic by a one-step hydrothermal synthesis. Systematic study of the optical and structure properties of CDs is presented in the work. In comparison to CDs prepared by other natural materials such as grass, potato, pomelo peel, willow bark, and waste biomass which have relatively low content of N and S elements, the QY of our CDs exhibited nearly double increase. The as-synthesized CDs can be applied in sophisticated and harsh conditions because of their excellent stability in a wide range of pH values and high ion strength solutions. Selective fluorescence quenching of CDs qualifies them as a probe to detect Fe^{3+} ion.

Methods

Materials

Fresh garlic were purchased from local supermarket (Changchun, Jilin Province). Ethylenediamine (EA) was attained from Aladdin. $Na_2S{\cdot}9H_2O$ were purchased from Xi Long Chemical Reagent Co., Ltd. Na_2SO_4, NaCl, KCl, $AlCl_3$, $ZnCl_2$, $Ba(NO_3)_2$, $FeCl_3$, $MgCl_2$, $Ni(NO_3)_2{\cdot}6H_2O$, $MnCl_2{\cdot}4H_2O$, $CuCl_2{\cdot}2H_2O$,$PbCl_2$, and $HgCl_2$ were obtained from Sinopharm Chemical Reagent Co., Ltd. and used without further purification.

Preparation of CDs

The garlic were peeled and washed and cut into small pieces and set in the oven at 50 °C for 24 h. After dehydration, the garlic pieces were ground into fine powder in a mortar; 0.5 g of garlic powder and 10 mL of deionized water were added in an autoclave with a polytetrafluoroethylene (PTFE) inner chamber and heated at 200 °C for 6 h (for N- and S-rich CDs, additional EA, $Na_2S{\cdot}9H_2O$ and Na_2SO_4 were added into the reaction). After the reaction, the autoclave was cooled to room temperature naturally. The reaction product was centrifuged at 5000 rpm for 10 min to remove the black precipitates, and then, the resulted supernatant was purified by filtering out large-sized carbon nanoparticles using a syringe filter with pores of 0.22 μm. Finally, the product was subjected to dialysis (MWCO = 1000 Da) in order to obtain the pure CDs.

Characterization

Fluorescence emission spectral measurements were carried out using a Shimadzu RF-5301 fluorescence spectrophotometer. Absorbance spectra were acquired by using a Shimadzu UV-3600 spectrophotometer. The surface morphology of the as-prepared CDs was investigated using a transmission electron microscope (TEM) (JEOL). X-ray diffraction (XRD) patterns of CDs were obtained using a Bruker D8 Advance X, Pert diffractometer (Cu Kα: λ = 1.5406 Å), in the range of 10°–70° at a scan rate of $4°min^{-1}$. Atomic force microscopy (AFM) images were recorded with a Veeco DI-3100 instrument. Fourier transform infrared spectroscopy (FTIR) was performed on an FTIR spectrophotometer (IFS-66 V/S). X-ray photoelectron spectroscopy (XPS) was conducted on an ESCALAB250 spectrometer. Binding energy of C 1 s at 284.7 eV was set as the calibration. The absolute PL QYs of the solution sample were measured by a fluorescence spectrometer (FLS920P, Edinburgh Instruments) equipped with an integrating sphere with its inner face coated with BENFLEC.

Metal Ion Detection of the CDs

Many different kinds of metal cations have been applied for the detection, such as Na^+, K^+, Al^{3+}, Zn^{2+}, Ba^{2+}, Fe^{3+}, Mg^{2+}, Ni^{2+}, Mn^{2+}, Cu^{2+}, Pb^{2+}, and Hg^{2+}. Briefly, a metal salt aqueous solution (250 μM, 2 mL) was mixed with a CD solution (0.05 mg/mL, 2 mL). After the mixture was vibrated for 5 min, the fluorescence spectra of the mixture were recorded.

pH Stability of CDs

HCl (2 M) or NaOH (2 M) was used to adjust the pH of the resultant CD solution (0.05 mg/mL, 2 mL), and the mixed solution was vibrated for 5 min. Then, the fluorescence spectra of the mixture were carried out.

Ion Strength Stability of CDs

NaCl aqueous solution (2 mL) with certain concentrations was mixed with a solution of CDs (0.05 mg/mL, 2 mL). Then, the fluorescence spectra of the mixture were recorded after the mixed solution was equilibrated for 5 min with vibrating.

Results and Discussion

Garlic is a natural world-wide edible condiment which is abundant in carbon, sulfur, and nitrogen elements and thus was used here as carbon source to synthesize the N- and S-doped CDs by a one-step hydrothermal treatment. After hydrothermal reaction, a light brown aqueous solution was produced indicating successful carbonization of the garlic. As shown in Fig. 1a, the CDs had roughly spherical shapes and were well dispersed with diameters in the range of 1–3 nm, which was supported by AFM results (Additional file 1: Figure S1a, c). Two broad peaks at 2θ of 25° and 44°can be seen from their XRD pattern (Additional file 1: Figure S1b), which is similar to other reported CDs [45]. In accordance with other reported CDs [39], the QY of CDs was enhanced from 5.1 to 10.5 %, while the emission wavelength and FWHM (full width at half maximum) were nearly the same with the increasing reaction temperature from 150 to 200 °C (Additional file 1: Table S1). The QYs of CDs prepared from different natural materials were shown in Additional file 1: Table S2. As can be seen, the QY of CDs doped with nitrogen and sulfur is better than grass, potato, pomelo peel, willow bark, and waste biomass which have relatively low content of nitrogen and sulfur.

The structure and components of CDs were identified by FTIR and XPS. As illustrated in Fig. 1b, the broad band at 3399~3283 cm^{-1} was attributed to O-H and N-H bonds [46]. A small band at 2931 cm^{-1} was ascribed to the C-H bonds [44]. The peak at 1769 cm^{-1} could be ascribed to C=O stretching vibration, while the peak at 1608 cm^{-1} was attributed to the C=C [27, 42]. Moreover, two bands at 1704 and 1454 cm^{-1} were assigned to the C=N and C–N stretching vibrations, respectively [42, 47]. In addition, the peak at 1121 cm^{-1} could be identified as the C–O, C–N, and C–S bonds [48] and the peak at 1048 cm^{-1} could be ascribed to $-SO^{3-}$, C–O–C, and C–O bonds [44, 49].

As Fig. 2a shows, four peaks with the binding energies of 532.0, 399.9, 284.8, and 168.3 eV can be observed, representing the presence of O 1s, N 1s, C 1s and S 2p, respectively. The high-resolution C1s spectrum in Fig. 2b has three peaks at 284.6, 286, and 288 eV, which were attributed to graphitic structure (sp^2 C=C), C–S, C–N, C–O (epoxy and alkoxy), and C=O species, respectively [27]. The N1s spectrum exhibited two main peaks (Fig. 2c), revealing the presence of both pyridinic N (400 eV) and pyrrolic N (401.7 eV) [27, 44], which was consistent with the FTIR results. According to Fig. 2d, the S 2p spectrum mainly consisted of three peaks centered at 164, 166, and 168.2 eV. The former two peaks could be attributed to $2p_{3/2}$ and $2p_{1/2}$ of the –C–S– covalent bond because of their spin-orbit couplings [44]. The latter peak could be deconvoluted into three components at 167.8, 168.1, and 169.3 eV, representing to the $-C-SO_x-$ ($x = 2, 3, 4$) species [44].

To further explore the optical properties of the CDs, absorption and photoluminescent (PL) spectra were studied as shown in Fig. 3. Absorption peak centered at 287 nm could be attributed to the presence of carbonyl or conjugated carbonyl groups. For the PL spectra, the optimal emission wavelength of CDs was centered at 426 nm with the excitation of 340 nm, showing the excitation wavelength dependent emission, which is similar to other reported CDs (Fig. 3b) [31, 42, 44, 50]. The dual emissive peaks (385 and 409 nm) can be seen from the PL spectrum (black line) with the excitation of 300 nm. The emission peaked at 385 nm gradually disappears, with the excitation wavelength changing from 320 to 440 nm. According to the previous studies [21, 51], the emission peak can be divided/fitted into several individual peaks with different energies. Under the short wavelength excitation, the excitation energy is high enough to excite all the several individual peaks. However, with the increase of the excitation wavelength, the excitation energy is not sufficient to excite the high energy transitions. As shown in the inset of Fig. 3a, bright blue photoluminescence of CDs can be easily recognized by eyes under UV light (365 nm). The QY of the CDs in aqueous solution was 10.5 %, which is comparable to previous reports, too [31, 38, 40, 41, 50].

Heteroatom-doped CDs can modulate compositions and structures of CDs to enhance the optical and

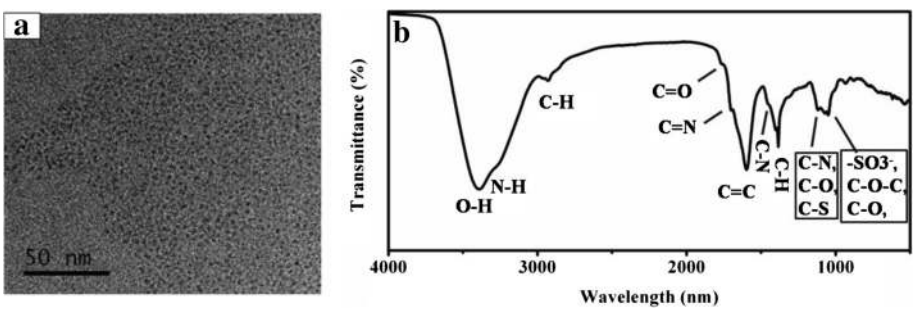

Fig. 1 TEM image and FT-IR spectrum of CDs. **a** TEM image of the CDs. **b** FT-IR spectrum of CDs

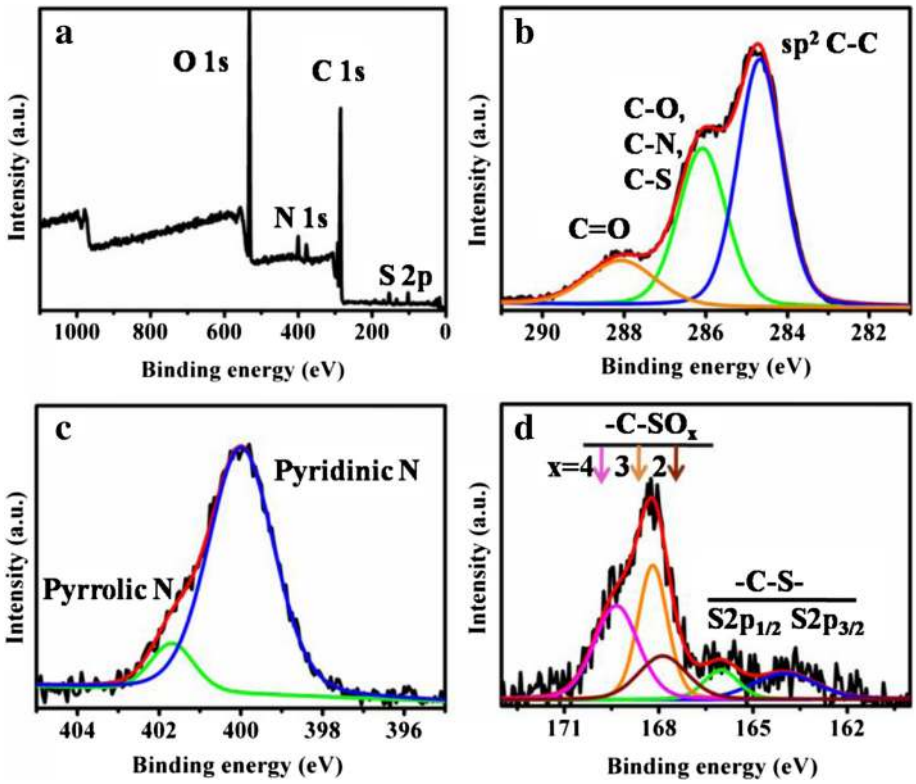

Fig. 2 XPS spectra of CDs. XPS spectra of CDs (**a**) and high-resolution spectra of C1s (**b**), N1s (**c**), and S 2p (**d**)

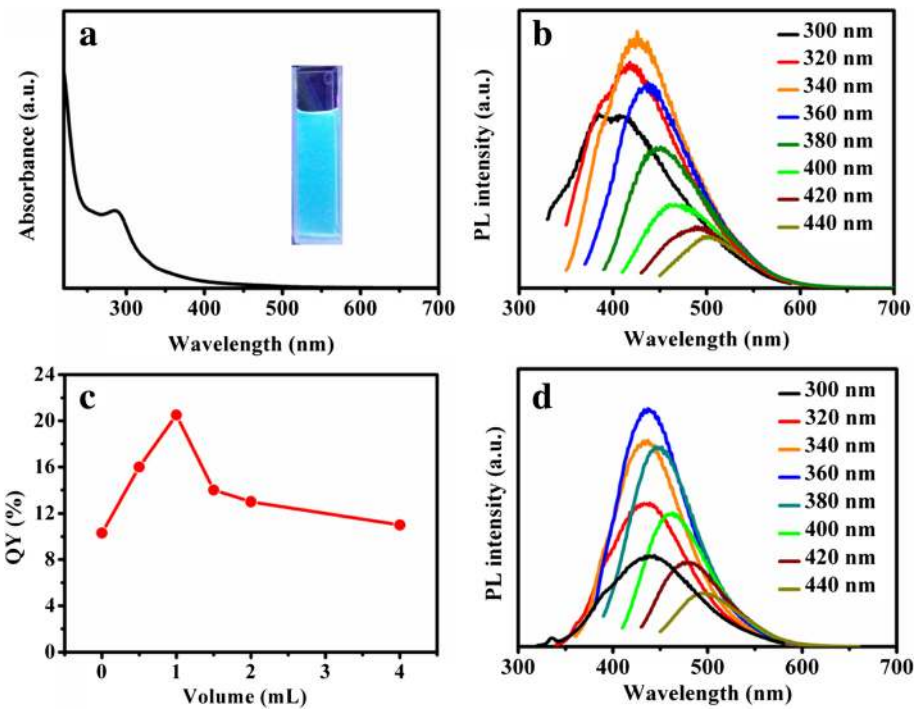

Fig. 3 Photoluminescence properties of CDs. **a** UV-vis absorption of CDs (*inset* was the photo under UV light). **b** PL emission spectra of CDs under different excitation wavelength from 300 to 440 nm. **c** PL QY of CDs prepared by adding different volumes of EA. **d** PL emission spectra of CDs with 1 mL EA added (CD-1) under different excitation wavelength from 300 to 440 nm

electronic properties [42, 43]. In order to elucidate the effect of N element and further increase the QY of the obtained CDs, an additional N-containing chemical was added into the hydrothermal synthesis. EA is a commonly used N precursor to synthesize N doped CDs, which was chosen in this work. In detail, different volumes of EA were added to the garlic powder and heated at 200 °C for 6 h. As shown in Fig. 3c, the QY firstly increased with the EA added and then dropped gradually with more EA. The highest QY could be tuned to 20.5 % with 1 mL of EA. When the ratio of EA was high, the CDs would be carbonized hardly [28] which led to lower QYs.

The absorption of two typical samples (1 mL EA denoted as CD-1 and 4 mL EA denoted as CD-4) was studied as shown in Additional file 1: Figure S2a. A new absorption band at 358 nm appeared for the EA addition, which is related to surface states [16, 27, 51]. Absorption and QY of CD-1 with different reaction times were shown in Additional file 1: Figures S2b and S3a. When the reaction time was 2 h, the absorption peak at 287 nm dominated and the QY was very low. However, when the reaction time was prolonged to 3 h, the absorption peak at 358 nm appeared and the QY was still not high. With the reaction time further prolonged, the absorption peaks remained unchanged. As shown in Additional file 1: Figure S3a, the QY firstly increased with the increase of reaction time up to 6 h; then, no apparent change of QY was observed with the reaction time to 8 h. Additional file 1: Figure S3b shows that the particle size of CD-1 was the same as that of the CDs without EA addition. The PL property of CD-1 was shown in Fig. 3d. The emission had a redshift of 10 nm compared to the one without EA.

The XPS and FTIR experiments were also carried out to identify the structure and components of these EA-assisted CDs. The band at 1769 cm^{-1} corresponding to C=O almost disappeared, and the bands at 1704 and 1454 cm^{-1}corresponding to C=N and C–N became more obvious in the FTIR spectra of CD-1 and CD-4 (Additional file 1: Figure S4), suggesting that N atom gradually substituted O atom during the dehydrolysis process, which was consistent with the elemental compositions result (Additional file 1: Table S3). The content of pyrrole N of CD-1 was higher than that of CD-4 which could be seen from Additional file 1: Figures S5 and S6. No other states of N and distinct differences were observed in the XPS, which proved that N atoms entered CD framework through the dehydrolysis and the content of N was helpful to acquire high QY.

Based on the above results, the role of EA in the synthesis of CDs could be explained as below. Firstly, the –COOH or the C=O, C–O of the garlic may react with EA, facilitating dehydrolysis and carbonization process. Then N atoms substitute part of O atoms to form amides, which leads to a newly formed surface state induced by N atoms. In this case, surface passivation may facilitate a high yield of the radiative recombination and depress the non-radiative recombination [52]. As a consequence, the PL QY of the resulting CDs increases as the N content of CDs increases.

Compared to the role of N, S shows relatively weak influence. Firstly, $Na_2S{\cdot}9H_2O$ was used as the S precursor to synthesize S-doped CDs. However, as shown in Additional file 1: Figure S7a, the QY of the CDs was not enhanced; conversely, the QY of the CDs declined with the increasing mass of S precursor. This is mainly because Na_2S is a strong base which has an effect on the PL intensity of the CDs. Then Na_2S was substituted by Na_2SO_4 whose pH was neutral. As shown in Additional file 1: Figure S7b, the QY of the CDs increased slightly with the increasing mass of S precursor, which is not as effective as the N precursor. The absorption and PL spectra of two S precursors were studied as shown in Additional file 1: Figure S8. For the Na_2S case, the absorption was the same to the one without S precursor when the amount of Na_2S was small. However, with the increasing of Na_2S amount, the absorption peak became less clear and changed as the absorption of CDs in pH value of 13. This is mainly because Na_2S is a base which could change the pH value of the reaction solution and led to the decline of PL intensity. The absorption did not change with the addition of the Na_2SO_4, indicating no energy level changed. The PL spectra of these two S precursors were the same, and a little difference was achieved from the CDs without S. Therefore, compared to the N precursor, the S precursors have inconspicuous influence on the dehydrolysis and carbonization process.

The pH behavior of the CDs was explored (Fig. 4). The CDs had high stability against pH variation in the range of 3–12. As illustrated in Fig. 4c, in aqueous solution with high pH 13, the absorption peak became less clear and exhibited an obvious red-shift by comparison with the CDs of pH 1 which gave rise to the color change of CDs under daylight (Fig. 4d). The carboxyl group on the surface of CDs turned to electronegative with higher pH, which could lead to the change of the absorption peak [53].

The influence of different ionic strengths on the PL intensity of CDs was also evaluated in NaCl solution with varying concentrations from 0 to 2.0 M. As shown in Fig. 5a, there are nearly no changes in either the PL intensities or the peak characteristics, which is beneficial to use these CDs in salt solutions such as buffers. The stability of the CDs in salt and wide pH conditions ensures that they can be applied in sophisticated and harsh conditions. Additionally, no obvious photobleaching phenomenon was observed with a continuous exposure

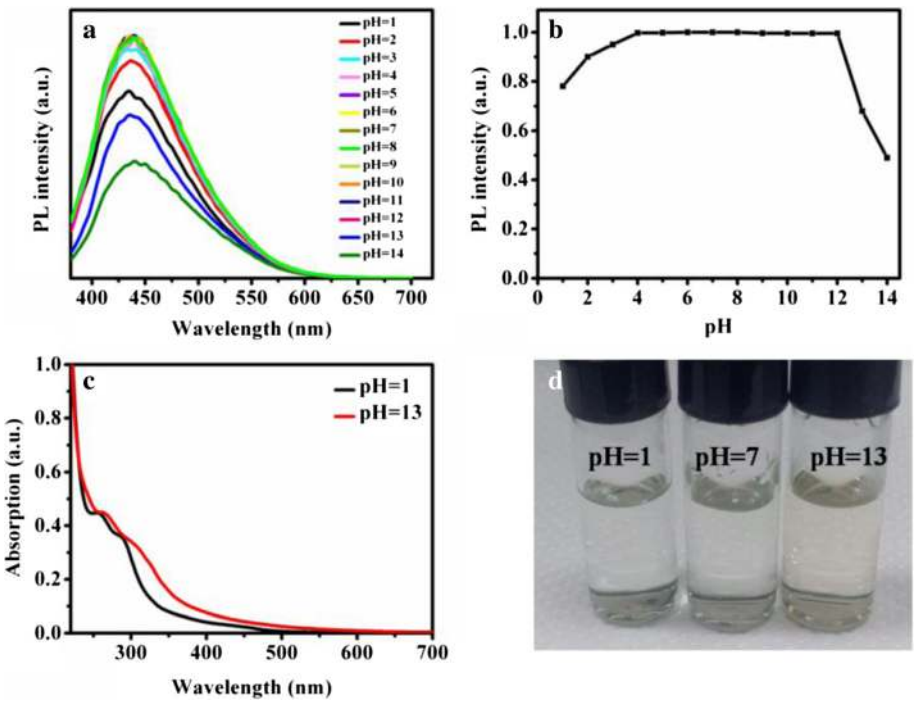

Fig. 4 The effect of pH for the CDs. **a** PL spectra for various pH in the range 1–14. **b** The PL intensity of pH variation. **c** The absorption spectra of CDs in aqueous solution under pH = 1 and 13. **d** The photographs of CDs under room light at pH = 1, 7, and 13

under UV excitation for 24 h, indicating excellent photostability of these CDs.

Recently, selective detection of metal ions using fluorescence materials has been the subject of many studies [31, 38, 39, 43, 50, 54]. The selective metal detection of CDs was monitored in the presence of different metal ions as shown in Fig. 6b. Obviously, Fe^{3+} ion showed the obvious fluorescence quenching effect on CDs, while the influence of other metal ions was almost negligible because the exceptional coordination between Fe^{3+} ion and hydroxyl group of CDs [31, 43, 50]. The fluorescence quenching effect of Fe^{3+} was performed to explore the sensitivity of CDs toward Fe^{3+} ion concentration. As shown in Fig. 6c, fluorescence intensity decreased with increasing Fe^{3+} concentration. Fig. 6d further represents the relation of the relative intensity $((F_0–F)/F)$ with different Fe^{3+} concentrations. The fluorescence quenching efficiency can be further described by the Stern–Volmer plot with a perfect linear behavior (the linear correlation coefficient was 0.995) in the range of Fe^{3+} concentrations from 0 to 500 μM. The Stern–Volmer equation was thus achieved as $F_0/F = 1.035 + 0.008\ [Fe^{3+}]$, where F_0 and F were the fluorescence intensities of CDs in the absence and presence of Fe^{3+} and $[Fe^{3+}]$ represented the concentration of Fe^{3+}. The detection limit was as low as 0.2 μM based on the calculation of $3\sigma/m$, where σ was the standard

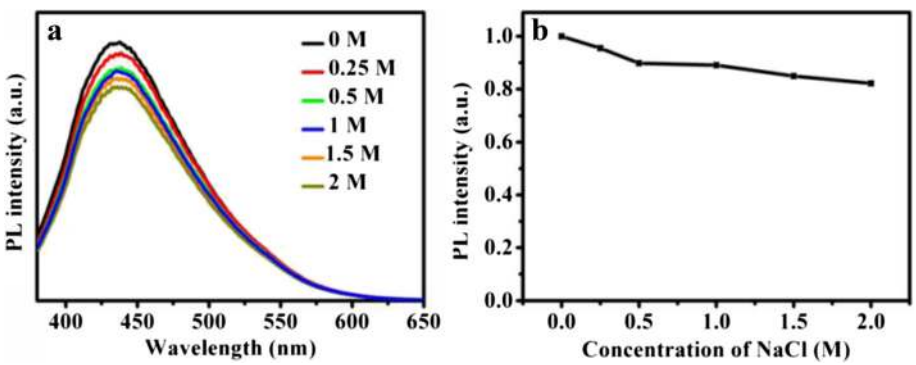

Fig. 5 The effect of ion strength for the CDs. **a** PL spectra in NaCl solutions with different concentrations; **b** the plot of PL intensity with NaCl variation

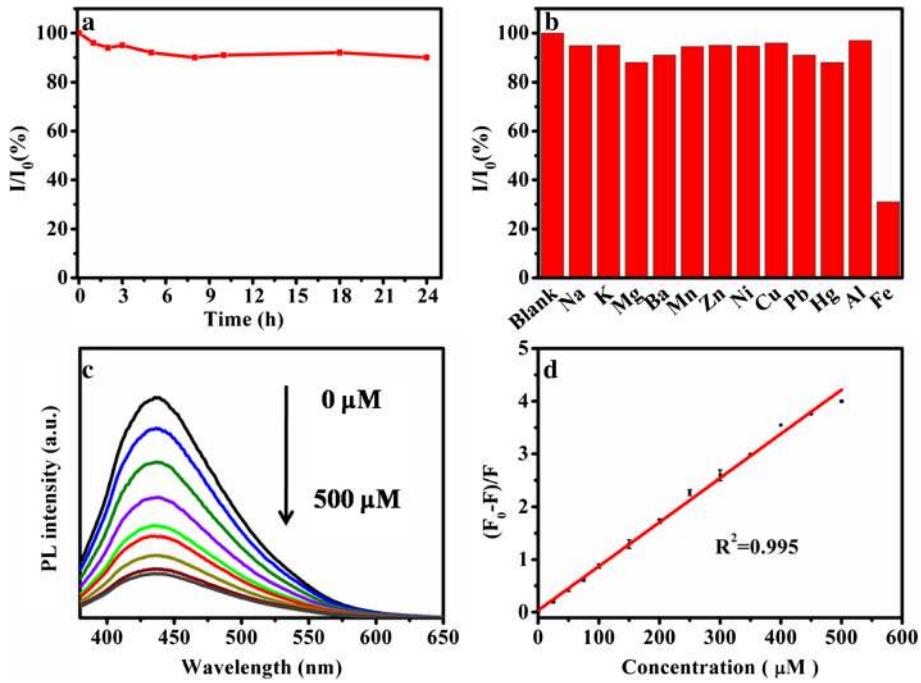

Fig. 6 Photostability and ion detection for CDs. **a** Photostability of CDs under UV excitation at various time. **b** The metal stability of CDs in the presence of different metal ions with the concentration of 250 μM. **c** PL spectra of CDs with different Fe^{3+} concentrations (0 to 500 μM). **d** Plot of $(F_0–F)/F$ with different Fe^{3+} concentrations (0 to 500 μM)

deviation of blank sample signal and *m* was the slope of the linear fit. Additional file 1: Table S4 shows the comparison of Fe^{3+} detection with different CDs. As can be seen, the detecting limit of 0.2 μM compares favorably with those of previous reports for Fe^{3+} detection [31, 43, 55, 56].

Conclusions

A direct, simple, and green synthetic approach for CDs using garlic as carbon source was presented. The content of N and the formation of C–N, C=N were critical to improve the PL QY. The as-prepared CDs showed no obvious photobleaching toward UV light. Fluorescence quench effect of the CDs in the presence of Fe^{3+} ion provided a platform for detecting Fe^{3+} ion from 0.2 to 500 μM.

Additional file

Additional file 1: Figures S1–S8 and Tables S1–S4. Figures depicting AFM and XRD (Figure S1), absorption of different volume of EA and different reaction time (Figure S2), QY of different reaction time and TEM of CD-1 (Figure S3), FTIR of CD-1 and CD-4 (Figures S4), XPS spectra of CD-1 and CD-4 (Figures S5 and 6), QY of different amount of S source (Figures S7), absorption and PL of S source (Figures S8), different reaction temperature (Table S1), comparison of different natural materials (Table S2), elemental compositions (Table S3), comparison of Fe^{3+} detection (Table S4)(DOC 2718 kb)

Competing interests

The authors declare that they have no competing interests.

Authors' contributions

CS conducted most of the experiments. PW and YY performed the XPS analysis and ion detection measurement, respectively. JX performed the FTIR measurement. CS, YW, and WWY designed the experiment. YZ and YW who are the corresponding authors participated in the overall experiments and revised the manuscript. All authors read and approved the final manuscript.

Acknowledgements

This work was financially supported by the National Natural Science Foundation of China (51272084, 61306078, 61225018, 61475062), the Jilin Province Key Fund (20140204079GX), the Opened Fund of the State Key Laboratory on Integrated Optoelectronics (IOSKL2013KF17), the Ministry of Education, Youth and Sports of the Czech Republic (LO1305), and the funding from Palacky University institutional support.

Author details

[1]State Key Laboratory on Integrated Optoelectronics, and College of Electronic Science and Engineering, Jilin University, Changchun 130012, China. [2]Department of Physical Chemistry, Regional Centre of Advanced Technologies and Materials, Faculty of Science, Palacký University in Olomouc, Šlechtitelů 27, 783 71 Olomouc, Czech Republic. [3]State Key Laboratory of Superhard Materials, and College of Physics, Jilin University, Changchun 130012, China. [4]Department of Engineering Science and Mechanics, The Pennsylvania State University, University Park, Pennsylvania 16802, USA.

Received: 28 October 2015 Accepted: 22 February 2016
Published online: 29 February 2016

References

1. Chen X, Nam S-W, Kim G-H, Song N, Jeong Y, Shin I et al (2010) A near-infrared fluorescent sensor for detection of cyanide in aqueous solution and its application for bioimaging. Chem Commun 46(47):8953–5

2. Santra S, Yang H, Holloway PH, Stanley JT, Mericle RA (2005) Synthesis of water-dispersible fluorescent, radio-opaque, and paramagnetic CdS:Mn/ZnS quantum dots: a multifunctional probe for bioimaging. J Am Chem Soc 127(6):1656–7
3. Zhang X, Zhang Y, Yan L, Ji C, Wu H, Wang Y et al (2015) High photocurrent PbSe solar cells with thin active layers. J Mater Chem A 3(16):8501–7
4. Tyrakowski CM, Snee PT (2014) A primer on the synthesis, water-solubilization, and functionalization of quantum dots, their use as biological sensing agents, and present status. Phys Chem Chem Phys 16(3):837–55
5. Yan L, Zhang Y, Zhang T, Feng Y, Zhu K, Wang D et al (2014) Tunable near-infrared luminescence of PbSe quantum dots for multigas analysis. Anal Chem 86(22):11312–8
6. Hu W, Henderson R, Zhang Y, You G, Wei L, Bai Y et al (2012) Near-infrared quantum dot light emitting diodes employing electron transport nanocrystals in a layered architecture. Nanotechnology 23(37):375202
7. Gu P, Zhang Y, Feng Y, Zhang T, Chu H, Cui T et al (2013) Real-time and on-chip surface temperature sensing of GaN LED chips using PbSe quantum dots. Nanoscale 5(21):10481–6
8. Yu WW, Qu L, Guo W, Peng X (2003) Experimental determination of the extinction coefficient of CdTe, CdSe, and CdS nanocrystals. Chem Mater 15(14):2854–60
9. Cademartiri L, Montanari E, Calestani G, Migliori A, Guagliardi A, Ozin GA (2006) Size-dependent extinction coefficients of PbS quantum dots. J Am Chem Soc 128(31):10337–46
10. Yu WW (2008) Semiconductor quantum dots: synthesis and water-solubilization for biomedical applications. Expert Opin Biol Th 8(10):1571–81
11. Liu W, Zhang Y, Wu H, Feng Y, Zhang T, Gao W et al (2014) Planar temperature sensing using heavy-metal-free quantum dots with micrometer resolution. Nanotechnology 25(28):285501
12. Katz E, Willner I (2004) Integrated nanoparticle-biomolecule hybrid systems: synthesis, properties, and applications. Angew Chem Int Ed 43(45):6042–108
13. Yu WW, Chang E, Drezek R, Colvin VL (2006) Water-soluble quantum dots for biomedical applications. Biochem Biophys Res Commun 348(3):781–6
14. Yu WW, Chang E, Falkner JC, Zhang J, Al-Somali AM, Sayes CM et al (2007) Forming biocompatible and nonaggregated nanocrystals in water using amphiphilic polymers. J Am Chem Soc 129(10):2871–9
15. Touceda-Varela A, Stevenson EI, Galve-Gasion JA, Dryden DTF, Mareque-Rivas JC (2008) Selective turn-on fluorescence detection of cyanide in water using hydrophobic CdSe quantum dots. Chem Commun 17:1998–2000
16. Sun C, Zhang Y, Wang Y, Liu W, Kalytchuk S, Kershaw SV et al (2014) High color rendering index white light emitting diodes fabricated from a combination of carbon dots and zinc copper indium sulfide quantum dots. Appl Phys Lett 104(26):261106
17. Wang Y, Kalytchuk S, Wang L, Zhovtiuk O, Cepe K, Zboril R et al (2015) Carbon dot hybrids with oligomeric silsesquioxane: solid-state luminophores with high photoluminescence quantum yield and applicability in white light emitting devices. Chem Commun 51(14):2950–3
18. Sun C, Zhang Y, Sun K, Reckmeier C, Zhang T, Zhang X et al (2015) Combination of carbon dot and polymer dot phosphors for white light-emitting diodes. Nanoscale 7(28):12045–50
19. Hola K, Zhang Y, Wang Y, Giannelis EP, Zboril R, Rogach AL (2014) Carbon dots—emerging light emitters for bioimaging, cancer therapy and optoelectronics. Nano Today 9(5):590–603
20. Sun C, Zhang Y, Kalytchuk S, Wang Y, Zhang X, Gao W et al (2015) Down-conversion monochromatic light-emitting diodes with the color determined by the active layer thickness and concentration of carbon dots. J Mater Chem C 3(26):6613–5
21. Zhang X, Zhang Y, Wang Y, Kalytchuk S, Kershaw SV, Wang Y et al (2013) Color-switchable electroluminescence of carbon dot light-emitting diodes. ACS Nano 7(12):11234–41
22. Baker SN, Baker GA (2010) Luminescent carbon nanodots: emergent nanolights. Angew Chem Int Ed 49(38):6726–44
23. Li H, Kang Z, Liu Y, Lee S-T (2012) Carbon nanodots: synthesis, properties and applications. J Mater Chem 22(46):24230–53
24. Hu S-L, Niu K-Y, Sun J, Yang J, Zhao N-Q, Du X-W (2009) One-step synthesis of fluorescent carbon nanoparticles by laser irradiation. J Mater Chem 19(4):484–8
25. Xu X, Ray R, Gu Y, Ploehn HJ, Gearheart L, Raker K et al (2004) Electrophoretic analysis and purification of fluorescent single-walled carbon nanotube fragments. J Am Chem Soc 126(40):12736–7
26. Bao L, Zhang Z-L, Tian Z-Q, Zhang L, Liu C, Lin Y et al (2011) Electrochemical tuning of luminescent carbon nanodots: from preparation to luminescence mechanism. Adv Mater 23(48):5801–6
27. Dong Y, Pang H, Yang HB, Guo C, Shao J, Chi Y et al (2013) Carbon-based dots co-doped with nitrogen and sulfur for high quantum yield and excitation-independent emission. Angew Chem Int Ed 52(30):7800–4
28. Zhu S, Meng Q, Wang L, Zhang J, Song Y, Jin H et al (2013) Highly photoluminescent carbon dots for multicolor patterning, sensors, and bioimaging. Angew Chem 125(14):4045–9
29. Tang L, Ji R, Cao X, Lin J, Jiang H, Li X et al (2012) Deep ultraviolet photoluminescence of water-soluble self-passivated graphene quantum dots. ACS Nano 6(6):5102–10
30. Li H, He X, Liu Y, Huang H, Lian S, Lee S-T et al (2011) One-step ultrasonic synthesis of water-soluble carbon nanoparticles with excellent photoluminescent properties. Carbon 49(2):605–9
31. Sachdev A, Gopinath P (2015) Green synthesis of multifunctional carbon dots from coriander leaves and their potential application as antioxidants, sensors and bioimaging agents. Analyst 140(12):4260–9
32. Zhai Y, Zhu Z, Zhu C, Ren J, Wang E, Dong S (2014) Multifunctional water-soluble luminescent carbon dots for imaging and Hg^{2+} sensing. J Mater Chem B 2(40): 6995–9
33. Wang L, Zhou HS (2014) Green synthesis of luminescent nitrogen-doped carbon dots from milk and its imaging application. Anal Chem 86(18): 8902–5
34. Lu W, Qin X, Asiri AM, Al-Youbi AO, Sun X (2012) Green synthesis of carbon nanodots as an effective fluorescent probe for sensitive and selective detection of mercury(II) ions. J Nanopart Res 15(1):1–7
35. Huang H, Xu Y, Tang C-J, Chen J-R, Wang A-J, Feng J-J (2014) Facile and green synthesis of photoluminescent carbon nanoparticles for cellular imaging. New J Chem 38(2):784–9
36. Barati A, Shamsipur M, Arkan E, Hosseinzadeh L, Abdollahi H (2015) Synthesis of biocompatible and highly photoluminescent nitrogen doped carbon dots from lime: analytical applications and optimization using response surface methodology. Mat Sci Eng C 47:325–32
37. Sahu S, Behera B, Maiti TK, Mohapatra S (2012) Simple one-step synthesis of highly luminescent carbon dots from orange juice: application as excellent bio-imaging agents. Chem Commun 48(70):8835–7
38. Lu W, Qin X, Liu S, Chang G, Zhang Y, Luo Y et al (2012) Economical, green synthesis of fluorescent carbon nanoparticles and their use as probes for sensitive and selective detection of mercury(II) ions. Anal Chem 84(12):5351–7
39. Liu S, Tian J, Wang L, Zhang Y, Qin X, Luo Y et al (2012) Hydrothermal treatment of grass: a low-cost, green route to nitrogen-doped, carbon-rich, photoluminescent polymer nanodots as an effective fluorescent sensing platform for label-free detection of Cu(II) ions. Adv Mater 24(15):2037–41
40. Qin X, Lu W, Asiri AM, Al-Youbi AO, Sun X (2013) Green, low-cost synthesis of photoluminescent carbon dots by hydrothermal treatment of willow bark and their application as an effective photocatalyst for fabricating Au nanoparticles-reduced graphene oxide nanocomposites for glucose detection. Catal Sci Technol 3(4):1027–35
41. Park SY, Lee HU, Park ES, Lee SC, Lee J-W, Jeong SW et al (2014) Photoluminescent green carbon nanodots from food-waste-derived sources: large-scale synthesis, properties, and biomedical applications. ACS Appl Mater Interfaces 6(5):3365–70
42. Ding H, Wei J-S, Xiong H-M (2014) Nitrogen and sulfur co-doped carbon dots with strong blue luminescence. Nanoscale 6(22):13817–23
43. Xu Q, Pu P, Zhao J, Dong C, Gao C, Chen Y et al (2015) Preparation of highly photoluminescent sulfur-doped carbon dots for Fe(III) detection. J Mater Chem A 3(2):542–6
44. Sun D, Ban R, Zhang P-H, Wu G-H, Zhang J-R, Zhu J-J (2013) Hair fiber as a precursor for synthesizing of sulfur- and nitrogen-co-doped carbon dots with tunable luminescence properties. Carbon 64:424–34
45. Mohapatra S, Sahu S, Sinha N, Bhutia SK (2015) Synthesis of a carbon-dot-based photoluminescent probe for selective and ultrasensitive detection of Hg^{2+} in water and living cells. Analyst 140(4):1221–8
46. Jiang J, He Y, Li S, Cui H (2012) Amino acids as the source for producing carbon nanodots: microwave assisted one-step synthesis, intrinsic photoluminescence property and intense chemiluminescence enhancement. Chem Commun 48(77):9634–6
47. Zhou J, Yang Y, Zhang C-y (2013) A low-temperature solid-phase method to synthesize highly fluorescent carbon nitride dots with tunable emission. Chem Commun 49(77):8605–7

48. Wang J, Wang C-F, Chen S (2012) Amphiphilic egg-derived carbon dots: rapid plasma fabrication, pyrolysis process, and multicolor printing patterns. Angew Chem Int Ed 51(37):9297–301
49. Peng H, Travas-Sejdic J (2009) Simple aqueous solution route to luminescent carbogenic dots from carbohydrates. Chem Mater 21(23):5563–5
50. Huang H, Li C, Zhu S, Wang H, Chen C, Wang Z et al (2014) Histidine-derived nontoxic nitrogen-doped carbon dots for sensing and bioimaging applications. Langmuir 30(45):13542–8
51. Wang Y, Kalytchuk S, Zhang Y, Shi H, Kershaw SV, Rogach AL (2014) Thickness-dependent full-color emission tunability in a flexible carbon dot ionogel. J Phys Chem Lett 5(8):1412–20
52. Qu D, Zheng M, Zhang L, Zhao H, Xie Z, Jing X et al (2014) Formation mechanism and optimization of highly luminescent N-doped graphene quantum dots. Sci Rep 4:5294
53. Wang C, Xu Z, Cheng H, Lin H, Humphrey MG, Zhang C (2015) A hydrothermal route to water-stable luminescent carbon dots as nanosensors for pH and temperature. Carbon 82:87–95
54. Tian J, Liu Q, Asiri AM, Sun X, He Y (2015) Ultrathin graphitic C3N4 nanofibers: hydrolysis-driven top-down rapid synthesis and application as a novel fluorosensor for rapid, sensitive, and selective detection of Fe^{3+}. Sens Actuators B 216:453–60
55. Qu K, Wang J, Ren J, Qu X (2013) Carbon dots prepared by hydrothermal treatment of dopamine as an effective fluorescent sensing platform for the label-free detection of iron(III) ions and dopamine. Chemistry – A European Journal 19(22):7243–9
56. Zhu W, Zhang J, Jiang Z, Wang W, Liu X (2014) High-quality carbon dots: synthesis, peroxidase-like activity and their application in the detection of H_2O_2, Ag^+ and Fe^{3+}. RSC Advances 4(33):17387–92